Desalination and Water Treatment
www.deswater.com

doi:10.5004/dwt.2017.0469

69 (2017) 130–141
March

Capacitive deionization of aqueous solutions: modeling and experiments

Yury M. Volfkovich[a], Daniil A. Bograchev[a,b,*], Alexey A. Mikhalin[a], Alexey Yu. Rychagov[a], Valentin E. Sosenkin[a], Daewook Park[c]

[a]*A. N. Frumkin Institute of Physical Chemistry and Electrochemistry, Russian Academy of Science, Leninskii prospect 31, 119071 Moscow, Russia, emails: yuvolf40@mail.ru (Y.M. Volfkovich), bograchev@gmail.com (D.A. Bograchev), almikh1985@gmail.com (A.A. Mikhalin), rychagov69@mail.ru (A.Y. Rychagov), vsosenkin@mail.ru (V.E. Sosenkin)*
[b]*National Research University Higher School of Economics (HSE), ul. Tallinskaya 34, Moscow, 123458 Russia, email: bograchev@gmail.com*
[c]*Samsung Raemian Apt. 102-201 Dongtanjiseong-ro 333 Hwaseong-si, Gyeonggi-do, Korea, email: park@samsung.com*

Received 27 April 2016; Accepted 28 July 2016

ABSTRACT

Capacitive deionization of $NaHCO_3$, KCl, $CaCl_2$, $MgSO_4$ solutions is studied under dynamic conditions. An electrochemical cell containing activated carbon electrodes is used. A two-dimensional model of this cell based on the model of a static cell is developed. The model takes into consideration ion adsorption-desorption and transport, surface conductivity of electrodes, electric double layer capacitance, as well as characteristics of the porous structure of the electrodes and separator obtained using the method of standard contact porosimetry. Characteristics of the deionization processes are shown to depend on the structure of the electric double layer. The time evolutions of fields of solution concentration were calculated from process beginning. The results are in agreement with experimental data which supports the model. This allows determining the optimal conditions for deionization processes. It is shown that both deionization and concentration are enhanced at an increase in voltage and at a decrease in the solution flow rate. The possibility of obtaining very pure water is determined by surface conductivity of the electrodes. The maximal deionization degree of 82% has been achieved for the 0.005 M KCl solution. The influence of the porous structure and hydrophilic-hydrophobic properties of the electrodes on characteristics of the deionization processes has been established.

Keywords: Capacitive deionization of water; Electric double layer; Surface conductivity; Method of standard contact porosimetry; Mathematical modeling

1. Introduction

Capacitive deionization (CDI) is a new promising electrochemical method of water desalination. Economically, it is the most attractive technique in comparison with reverse osmosis, distillation and electromembrane separation [1,2]. As opposed to electrodeionization involving ion exchange membranes and an ion-exchanger bed between them [3–6], electrodes play the key role in CDI processes.

CDI involves the passing of aqueous solution through the electrochemical cell between two highly dispersive carbon electrodes (HDCE) with a high specific surface area (≈500–2,500 m^2 g^{-1}) [1,2], between which a potential difference (>1.2 V) is applied. Adsorption of anions and cations occurs on positively and negatively charged electrodes, respectively; the electric double layer (EDL) is charged similarly to that in supercapacitors. This results in deionization of the solution. When the circuit is closed or polarity is reversed, ions diffuse from the solid–liquid

*Corresponding author.

Presented at the EDS conference on Desalination for the Environment: Clean Water and Energy, Rome, Italy, 22–26 May 2016.

interface back to the solution. This causes an increase of the solution concentration and energy regeneration. The deionization stage corresponds to the charging of the electrochemical supercapacitor (ECSC), and the concentration (regeneration) stage is related to discharging. During the concentration stage, a significantly lower amount of water is supplied to the cell. After regeneration of the electrodes, the cell is converted to a deionization cell etc. The CDI device including at least two electrochemical cells operates continuously. While deionization takes place in the first cell, concentration occurs in the second cell. Two products are obtained: pure water and a concentrated solution. The concentrate can be used further for different purposes.

As opposed to reverse osmosis and nanofiltration, CDI does not requires high pressure, the equipment for this process (pipes, pumps) is less expensive [7]. Moreover, the applied cell voltage provides a high level of safety. The CDI method can be used in remote regions, since it is able to involve alternative energy sources, particularly solar batteries. The consumed energy can be partially compensated by electrical energy from the regeneration unit. As a result, the consumed energy is three times less than in the case of reverse osmosis. One other source of a decrease in the energy consumption is using HDC possessing high surface conductivity (SC; tangential EDL conductivity) [8]. These electrodes are characterized by long-term cyclability due to EDL reloading without faradaic reactions. The CDI device can operate under various flow rates and different levels of desalination.

The CDI processes are attractive for desalination of brackish and ground water, but are not recommended for removal of traces from complex solutions [9]. For instance, this technique can be also used at home for water softening in washing machines.

Electrode materials for CDI have been the focus of attention in the last years. Different types of both single-component (activated carbons, aerogels, nanotubes, graphenes etc.) [10–17] and carbon-based composite materials (carbon–carbon composite, carbon–metal oxide composite, carbon–polymer composite and carbon–polymer–metal oxide composite) [18–28] have been suggested. CDI application for removal of different salts from water has been investigated [29–33].

The CDI devices and conditions of deionization and concentration can be optimized by means of modeling the processes. A number of models for ESCs with HDCE accounting for the electrolyte transport along the electrodes and separator as well as the charging of EDL of the electrodes, has been developed [34,35]. However, hydrodynamic conditions were outside the models. Approaches considering EDL in a single pore have been suggested [36,26]. These models are invalid for low-concentration solutions: the thickness of the diffuse region of EDL is larger than the micropore radius (1–2 nm) providing the largest contribution to the specific surface area of HDCE. Hydrodynamic transport of electrolyte along the outer surface of the electrodes is also outside the models. In fact, a two-dimensional model is necessary for the CDI processes, since they involve porous electrodes. Some approaches take into consideration the electrolyte flux [37–39] or SC [40–42]. The method of SC measurements has been first proposed in [8] for porous electrodes. It should be stressed that the carbon materials are characterized by hydrophilic and hydrophobic porosity [43] not considered in the known models. The information about hydrophilicity-hydrophobicity can be obtained only using the method of standard contact porosimetry (MSCP) [44–46], which has been recognized by IUPAC [47].

The aim of the investigation was to develop the mathematical model of CDI processes and to confirm it experimentally. Another purpose was to establish the effect of EDL characteristics on deionization. The work involved the following tasks: (i) studies of the porous structure and hydrophilic-hydrophobic properties of AC-based HDCE, (ii) experimental and theoretical study of CDI in a static electrochemical cell without any solution flow (for estimation of deionization in pores of the electrodes and for measurements of their specific capacitance), (iii) experimental and theoretical study of operation of dynamic deionization cell with a flow of aqueous solution.

2. Experimental

2.1. Materials

Activated carbontextiles (ACT), suchasCH900 (Curaray Co, Japan), VISKUMAK (Neorganica LTD, RF) were applied in investigations, since these electrodes are characterized by a rather high specific surface area. Moreover, they are much more attractive from the economical point of view than other highly dispersive carbon materials, such as graphenes, nanotubes and carbide derived carbons used by many authors for CDI. The electrodes of the SAIT type (SAIT Co, Republic of Korea) were also used. These electrodes were manufactured by compaction of activated carbon powder in the presence of a binder (polytetrafluorethylene, PTFE).

2.2. Porosimetric measurements and morphology of electrodes

Since porous structure characteristics and hydrophilic-hydrophobic properties of AC electrodes affect the CDI process, the measurements using MSCP [44–47] were applied. This method allows studying the porous structure in a wide range of pore radii: from ~1 nm to 100 μm (5 orders of magnitude). As opposed to other porosimetric techniques, only MSCP provides estimation of hydrophilicity–hydrophobicity. Octane (determination of both hydrophilic and hydrophobic pores) and water (only for hydrophilic pores) were used as working liquids.

Morphology of the samples was studied using a JSM-U3 scanning electron microscope (JEOL, Japan) supplied with a DISS top box for digital scanning (GETAC, Germany).

2.3. CDI processes in static cell

Electrical capacitance of AC electrodes is a sum of EDL capacitance and pseudocapacitance of Faraday reactions [48–50]. Due to this, the electrode capacitance was measured; the EDL capacitance was calculated from this value and used further for simulation.

Galvanostatic measurements of dependences of cell voltage on time were carried out at 25°C under charging-discharging in order to determine the EDL capacitance. A static cell with the electrolyte present only in the pores of the electrode and separator was used. The cell design and methods of measurements are described in detail in [49]. The measurements at 0–1.5 V were performed using a Voltalab-40 potentiostat (Radiometer Analytical, France).

Single-component $NaHCO_3$, $CaCl_2$, and $MgSO_4$ solutions of different concentrations (100, 500 and 1,000 mg-eq dm^{-3}) as well as a mixed solution were used. A composition of the mixture was as follows (mg-eq dm^{-3}): $NaHCO_3$ (4.4), $CaCl_2$ (11.9), $MgSO_4$ (10.7). This composition corresponds to brackish water. The capacitance of the electrodes ($C_{c,full}$) was determined as:

$$C_{c,full} = \frac{2I_{full}\Delta t}{\Delta U} \quad (1)$$

where U is the cell voltage, I_{full} is the current, t is the time.

Since adsorption capacity of the electrodes is proportional to the EDL capacitance ($C_{EDL,full}$), a change in solution concentration (ΔC) during the process is expressed as:

$$\Delta c = \frac{C_{EDL,full}\Delta U}{2FV} \quad (2)$$

where F is the Faraday constant, V is the solution volume. It is assumed that the adsorption efficiency is 100% during the EDL charging. The Eq. (2) is also valid for electrodes of equal capacitance.

2.4. CDI processes in a dynamic electrochemical cell

Fig. 1 illustrates a scheme of a dynamic CDI device (Samsung Electronics Co.). A solution is supplied from the tank by means of a peristaltic pump. Further, the liquid is passed through a valve and a pressure sensor. Then the solution arrives at the cell, where deionization or concentration occurs. After the cell, the solution flows successively through the conductivity meter, pH meter and the second valve into the sink. Argon was purged through the system during the processes in order to remove oxygen from pores of the electrodes and separator.

In addition to the mixed solution of the above composition, a KCl solution (5 mg-eq dm^{-3}) was used. The values of its electrical conductivity can be easy recalculated to concentration, since reference data are available elsewhere for wide concentration and temperature ranges. The deionization degree was calculated as follows:

$$\frac{C_{in} - C_{min}}{C_{in}} \times 100\%$$

where C_{in} and C_{min} are the initial and minimal concentration of the solution.

3. Results and discussion

3.1. Porous structure of electrodes and separator

Fig. 2 illustrates SEM images of the electrodes. Fibers of the VISKUMAK material are rather ordered, their diameter is in the micron size. The fibers form intertwined bundles with the thickness of about 1,000 μm. The same structure has been found for the CH900 textile; however, the fibers are more disordered. Corpuscular structure is attributed to the SAIT composite, agglomerates of particles are visible.

It is found that pores of all investigated electrodes form a very wide range; their radius is from ~1 nm to 100 μm. All electrodes are characterized by both hydrophilic and hydrophobic porosity; the values of the effective wetting angle are close to 90°, especially for SAIT that contains an inert binder (Table 1). The specific surface area values are large and sufficiently different from each other. It is the same for hydrophilic and hydrophobic porosity.

The porous structure of the separator involves pores with the radius within the interval of 3–100 μm; the pores with the radius of 10 μm are prevailing. The total porosity of the separator is 0.8 cm^3cm^{-3}. Characteristics of the porous structure of both the electrodes and the separator were used further for the modeling of CDI processes.

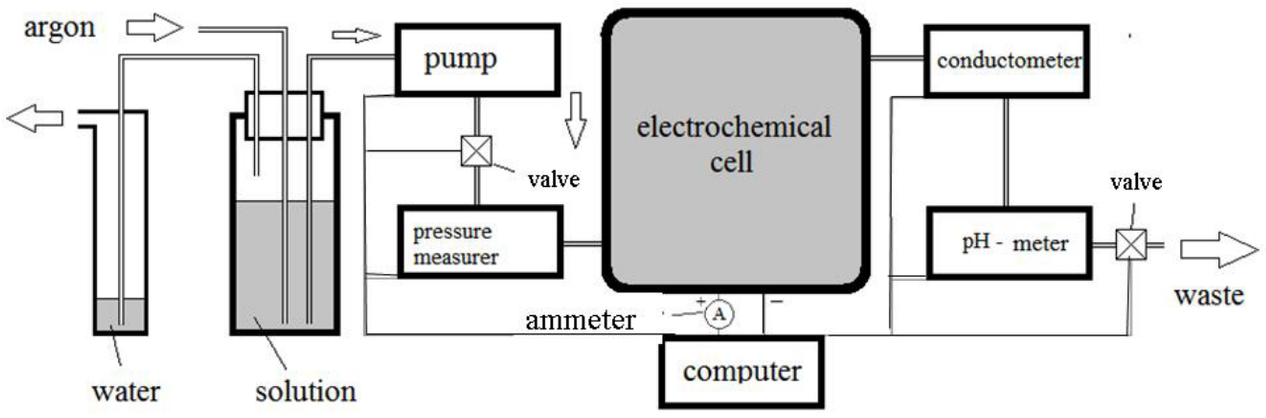

Fig. 1. Schemeofa dynamic CDI device.

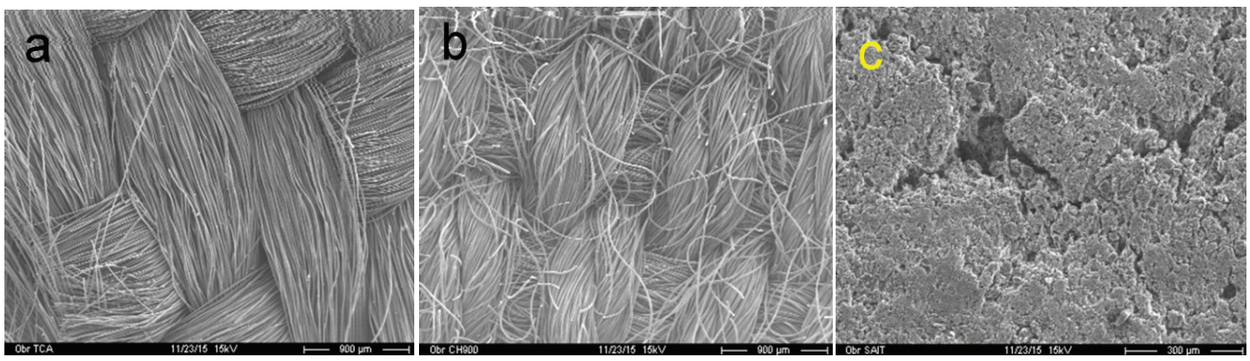

Fig. 2. SEM images of the (a) VISKUMAK, (b) CH900 and (c) SAIT electrodes.

Table 1
Structure characteristics of AC electrodes

Electrode	Specific surface area ($m^2\ g^{-1}$)		Porosity ($cm^3 cm^{-3}$)			Average wetting angle for hydrophilic pores
	Total	Hydrophilic	Total	Hydrophilic	Hydrophobic	
CH900	1520	850	0.851	0.786	0.064	77.5
SAIT	940	520	0.715	0.492	0.225	87.3
VISKUMAK	600	416	0.729	0.623	0.106	79.9

3.2. Processes in a static electrochemical cell

The CDI model requires also the values of specific EDL capacitance of electrodes obtained for different aqueous media. No theoretical solution of this problem has been proposed with respect to carbon electrodes containing both micro and macropores. In this work, the experimental method has been suggested that allows determining the EDL capacitance. The technique is based on measurements of electrochemical capacitance under various currents (i.e., under galvanostatic conditions) followed by calculations according to Eq. (1).

The typical curve of integral capacitance of the electrode vs. current density is shown in Fig. 3. The capacitance grows at a decrease in current density and then manifests a plateau followed by a further decrease. The build-up of capacitance in the region of high current density is due to significant ohmic losses under these conditions. The plateau corresponds to very low ohmic losses; the capacitance is affected only by EDL. At low currents, pseudocapacitance of faradaic processes influences the value of *C*. The faradaic processes are quasi-reversible redox reactions of the electrode surface groups [49].

It was suggested that the capacitance values of the plateau region corresponded to EDL capacitance per mass unit (C_{EDL}) in the first approximation. This value was divided by the hydrophilic surface area (see Table 1). The values of EDL capacitance per area unit (C^S_{EDL}) were obtained in this way. These data were further used in the modeling of CDI processes. The values of both C_{EDL} and C^S_{EDL} grow at an increase in the solution concentration evidently due to contraction of the diffuse region of the EDL (Tables 2 and 3). The EDL is realized in smaller pores under these conditions.

As found for single-component ACT electrodes, they show the highest capacitance in 1:1 electrolytes, namely in $NaHCO_3$ and KCl solutions. The smallest C_{EDL} and C^S_{EDL} values have been suggested for 2:2 electrolyte, such as $MgSO_4$. Regarding 1:2 electrolyte like $CaCl_2$, intermediate data have been obtained.

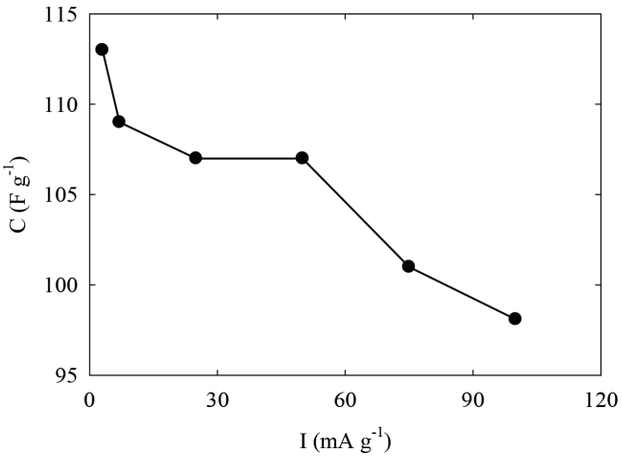

Fig. 3. Dependence of capacitance of the CH900 electrode on current density in a 1 N $CaCl_2$ solution.

Since the porous structure and hydrophilic-hydrophobic properties of the investigated electrodes are rather complex, it is difficult to explain clearly a relationship between their electrochemical characteristics. Nevertheless, it is possible to state the highest C_{EDL} value for the CH900 material, which is characterized by the largest hydrophilic surface area (see Table 1). These characteristics are the smallest for the SAIT composite, which demonstrates the lowest values of the EDL capacitance. Intermediate C_{EDL} values have been found for the VISKUMAK electrode.

Table 2
Values of C_{EDL} and C^S_{EDL} for different electrodes

Salt	c (mg-eq dm^{-3})	CH900		VISKUMAK		SAIT	
		C_{EDL} (F g^{-1})	C^S_{EDL} (μF cm^{-2})	C_{EDL} (F g^{-1})	C^S_{EDL} (μF cm^{-2})	C_{EDL} (F g^{-1})	C^S_{EDL} (μF cm^{-2})
KCl	100	84.6	9.95	72	17.5	5.2	10.1
$NaHCO_3$	100	80.6	9.48	69	16.6	50	9.6
	1,000	110.1	13.2	110.3	26.2		
$CaCl_2$	100	78.8	9.27	58.6	14.1		
	1,000	107.1	12.6	99.6	24.2	74.1	14.3
$MgSO_4$	100			55.4	13.3	47.5	9.1
	1,000	86.1	10.1	92.1	22.2		
Mixture	See Section 2.3	63.2	7.4				

Table 3
C_{EDL} and C^S_{EDL} magnitudes for the VISKUMAK electrodes

EDL capacitance	C_{NaHCO_3} (mg-eq dm^{-3})			C_{CaCl_2} (mg-eq dm^{-3})			C_{MgSO_4} (mg-eq dm^{-3})		
	100	500	1,000	100	500	1,000	100	500	1,000
C_{EDL} (F g^{-1})	69.0	94.8	110.3	58.6	74.5	99.6	55.4	67.3	92.1
C^S_{EDL} (μF cm^{-2})	16.6	22.8	26.2	14.1	18.0	24.2	13.3	16.0	22.2

3.3. Deionization in a dynamic cell

Investigations under dynamic conditions were performed in order to test the effect of experimental conditions on CDI processes involving electrodes of different porous structure and also to estimate energy efficiency of deionization and concentration. The dependencies of current on time were used further for comparison with theoretical data.

Typical plots reflecting a change in charging current and solution conductivity in time, are given in Fig. 4. When voltage is applied, the current rapidly increases and then gradually decreases due to the charging of EDL. This causes adsorption of species on the electrodes; the solution conductivity decreases. Discharging at $U = 0$ is accompanied by regeneration of the electrodes; this causes an increase in the solution conductivity. Further, the conductivity becomes close to the initial value.

In accordance with Eq. (2), deionization is affected by the applied cell voltage. For example, Fig. 5(a) shows conductivity of the mixed solution as a function of time when the SAIT electrodes were used. The maximal ratios of concentrations of the solutions at the cell inlet and outlet were 1.47–1.85 with the cell voltage varied from 1 to 1.6 V. An increase in voltage causes also improves concentration during discharging evidently due to an increase in the amount of ions adsorbed during charging.

In the case of a single-component KCl solution, the $\kappa - t$ plots for the CH900 electrodes were rearranged into the $C - t$ curves using reference data in order to obtain more visual information about CDI processes. Some results are given in Fig. 5(b). The deionization degree reaches 42%–79% in the same interval of voltage. The maximal concentration of the solution during discharging is five times higher than

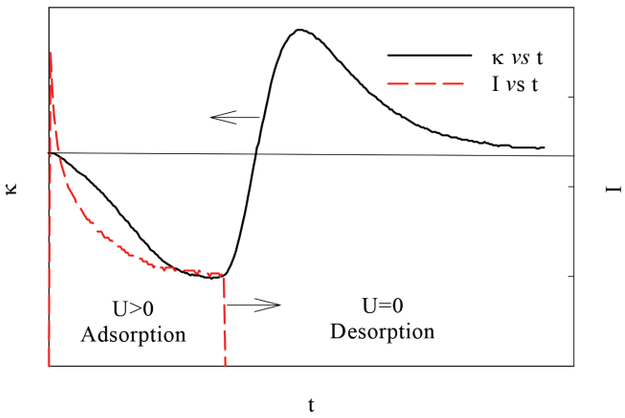

Fig. 4. Charging current and electrical conductivity of the solution through the cell vs. time.

the initial concentration, when adsorption at 1.6 V occurs. A further increase in voltage is undesirable as it may cause additional electrode reactions.

The following values were calculated on the basis of the results obtained for the solution containing initially 5 mg-eq dm^{-3} KCl (some data are given in Table 4): W_d (energy consumption of the deionization stage), W_c (energy recovery of the concentration stage), W_r (resulting deionization energy, $W_r = W_d - W_c$), χ (specific energy efficiency). The latter parameter is determined as the amount of salt (in our case, KCl) removed due to spending of 1 J.

The W_r energy must be taken into consideration during the operation of the CDI stack, since there is a gain due to

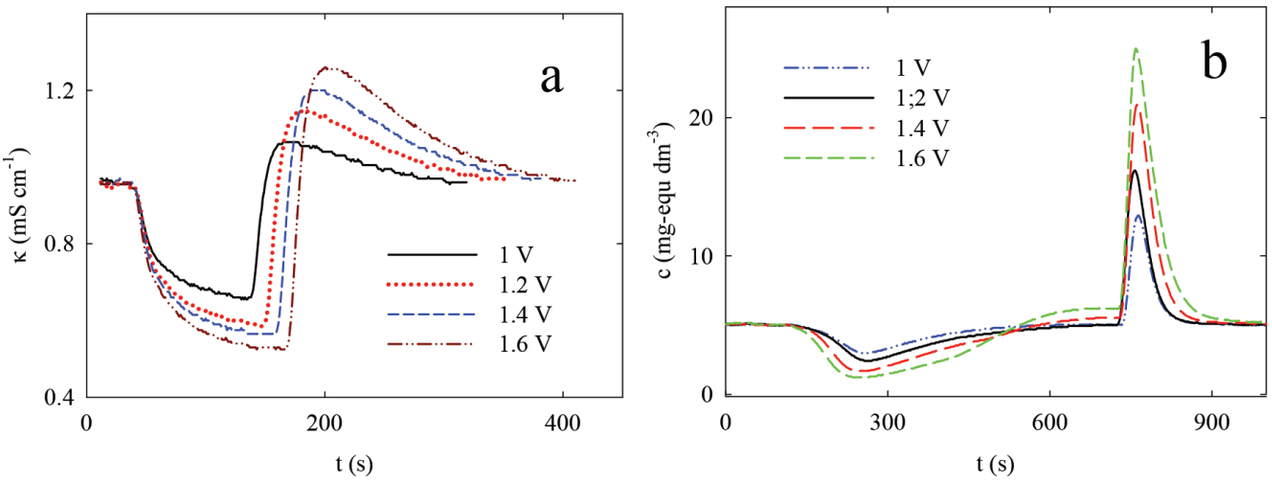

Fig. 5. Conductivity of mixed solution (a) and concentration of KCl solution (b) as functions of time. The SAIT (a) and CH900 (b) electrodes were used. The flow velocity of the solutions was 30 $cm^3 min^{-1}$.

Table 4
Deonization and concentration of the KCl solution (5 mg-eq dm^{-3}) in the first 600 s; the CH900 sample was used as electrodes

U (V)	20 $cm^3 min^{-1}$					30 $cm^3 min^{-1}$				
	W_d (J)	W_c (J)	Deionization degree (%)	W_r (J)	χ (mol J^{-1})	W_d (J)	W_c (J)	Deionization degree (%)	W_r (J)	χ (mol J^{-1})
1	230	–37	55	193	7.49×10^{-7}	289	–37	42	252	6.14×10^{-7}
1.2	564	–47	60	517	5.54×10^{-7}	485	–57	54	428	5.87×10^{-7}
1.4	735	–74	73	661	4.75×10^{-7}	675	–82	69	593	5.79×10^{-7}
1.6	1116	–94	82	1022	3.32×10^{-7}	897	–113	79	784	5.49×10^{-7}

the use of energy during the concentration stage, i.e., regeneration of the energy. This energy gain causes much lower energy consumption in CDI processes as compared with other techniques of water desalination. As shown in Table 4, increasing cell voltage and reducing the solution velocity cause an increase in the desalination degree. At the same time, the value of energy efficiency decreases due to ohmic losses. It is necessary to note, that the data on the deionization degree in Table 4 are sufficiently higher than the results obtained for the CDI processes involving graphene electrodes [15].

A possibility of multiple deionization-concentration of the mixed solution has been shown at the example of the VISKUMAK electrode (Fig. 6). Here the minimal and maximal concentrations of the solution are reproduced after each cycle. Moreover, differences in the initial-minimal concentrations and maximal-initial concentrations are practically equal. During deionization, a slight shift in pH was observed during the deionization stage probably due to the effect of surface groups of the electrodes, the deviation from the initial value became more insignificant from cycle to cycle.

It was also found that the highest degrees of deionization and concentration are obtained for the CH900 electrodes (Fig. 7), since they are characterized by the highest values of specific hydrophilic surface area and hydrophilic porosity (see Table 1). Hydrophilic surface determines the value

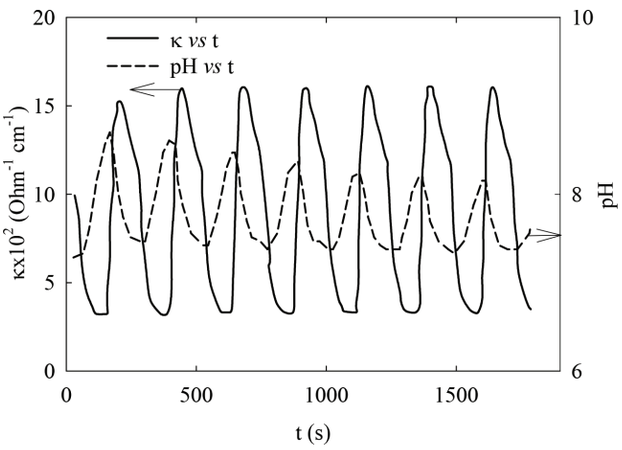

Fig. 6. Electrical conductivity and pH of the mixed solution as a function of time of multiple charging-discharging of the VISKUMAK electrodes. The solution flow velocity was 40 $cm^3 min^{-1}$, U = 1.25 V.

of EDL capacitance; hydrophilic porosity affects effective electrical conductivity according to the Archie's expression (see Section 3.4). The lowest degrees of deionization and concentration were obtained for the SAIT electrodes. Indeed, the smallest value of hydrophilic porosity has been

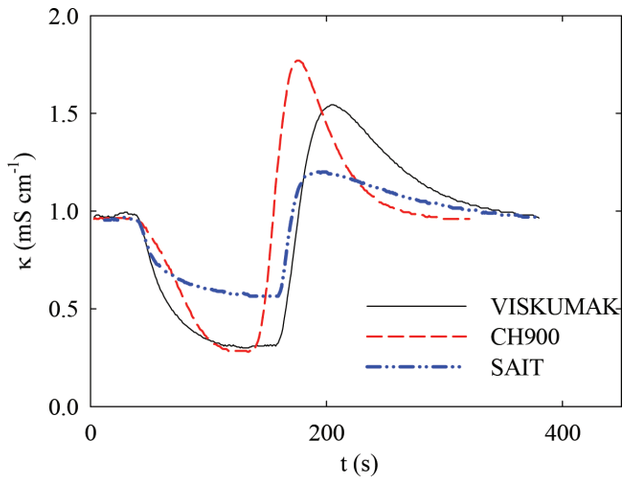

Fig. 7. Electrical conductivity of the mixed solution as a function of time for deionization (at 1.25 V) and concentration stages. Different electrodes were used. The solution flow velocity 20 $cm^3 min^{-1}$.

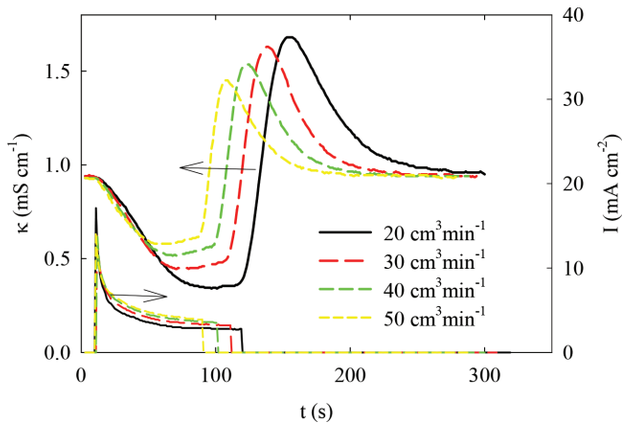

Fig. 8. Conductivity of the mixed solution and charging current as functions of time. CH900 electrodes were used, U = 1.25 V.

found for that material. Based on the obtained results, the CH900 electrodes were used for further investigations.

An increase in the flow rate impairs both deionization and concentration, but a slight growth of charging current is observed (Fig. 8). On the other hand, improvement of the process efficiency and reducing energy consumption can be achieved in this manner (see also Table 4).

In general, the data in this section show the importance of solution flow velocity for the modeling of CDI processes. Moreover, the electrodes with different hydrophilic-hydrophobic properties and different EDL capacitance manifest different behavior during deionization-concentration. These characteristics are to be taken into consideration for development of the models.

3.4. Mathematical modeling of charging-discharging under static conditions

Fig. 9 is a scheme of the model of the CDI cell with a simple 1D structure. The cell involves two porous carbon

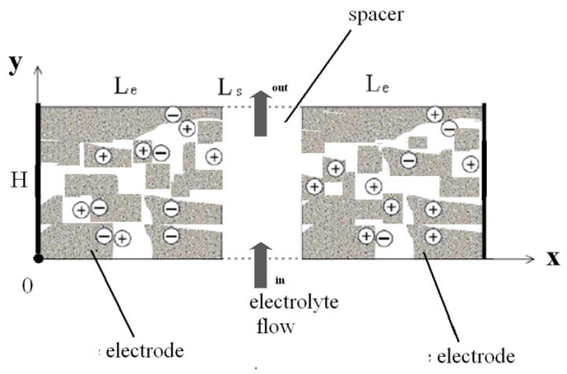

Fig. 9. Geometrical model of CDI cell.

electrodes and a porous separator (spacer) between them. A flow of the solution that is shown in the figure is outside this model, but it will be taken into consideration for the dynamic cell (see Section 3.5).

The following assumptions have been made. Resistance of the electrode was neglected due to its much higher conductivity as compared with the solution. The conductivity and diffusion coefficients were corrected according to the Archie's law for porous materials [51,52]:

$$\kappa = \kappa_1(c)\varepsilon^m; D = D_0\varepsilon^m \tag{3}$$

where ε is the porosity, $k_1(c)$ and D_0 are the conductivity of free electrolyte and its diffusion coefficient, m is the Archie's exponent. The last value reflects the effect of the porous structure on electrolyte transport [51–53]. The theory of a binary diluted solution [54] was used in the model for mass transport calculations:

$$\varepsilon\frac{\partial c}{\partial t} = D\frac{\partial^2 c}{\partial x^2} + \frac{C_s}{Fz_+}A_E\frac{\partial \varphi}{\partial t} \tag{4}$$

Here A_E is the electric adsorption coefficient, jis the electrical potential of electrolyte, C_s is the specific capacitance of electrode that becomes zero for the separator. The charge transport in the electrolyte is as follows:

$$C_s\frac{\partial \varphi}{\partial t} = \frac{\partial}{\partial x}\left(\kappa_{eff}\frac{\partial \varphi}{\partial x}\right) + \frac{\partial}{\partial x}\left(\frac{\kappa_E(t_+ - t_-)}{f}\frac{\partial \log c}{\partial x}\right) \tag{5}$$

where t_+ and t_- are the transport numbers of cations and anions respectively, κ_{eff} is the effective conductivity, $\kappa_{eff} = \varepsilon^m\kappa_0\frac{c}{c_0} + \kappa_s$, κ_E is coefficient assumed to be equal to zero (C_0 is the initial concentration, κ_0 is the electrolyte conductivity under initial concentration, κ_s is the SC) [8]. It is assumed, that the κ_s value is proportional to the amount of adsorbed ions:

$$\kappa_s = \sigma\frac{tI_{full}}{FV_{eff}} \tag{6}$$

where σ is the SC coefficient, t is the time, I_{full} is the full current, V_{eff} is the effective volume.

The task is solved for the porous electrode and half the separator (half the cell). The symmetry of the system with respect to boundary conditions is considered. On the left side ($x = 0$) and in the center of the separator ($x = L_e + \frac{1}{2}L_s$), the boundary conditions are:

$$\left.\frac{\partial c}{\partial x}\right|_{x=0} = 0;\ \left.\frac{\partial \varphi}{\partial x}\right|_{x=0} = 0 \left.\frac{\partial c}{\partial x}\right|_{x=L_e+\frac{1}{2}L_s} = 0;\ \kappa \left.\frac{\partial \varphi}{\partial x}\right|_{x=L_e+\frac{1}{2}L_s} = -\frac{I_{full}}{S} \quad (7)$$

The initial conditions are:

$$c = c_0;\ \varphi = 0 \quad (8)$$

Only specific adsorption is assumed to occur before charging; this results in a decrease in the initial concentration. The initial concentration was also a fitting parameter, its value was found by comparison of the theoretical and experimental data, as shown further.

System (4)-(6) with boundary conditions (7) and initial conditions (8) was solved using numerical methods. The system of equations is presented in a common form for all parts of model. It is assumed that diffusion, conductivity, porosity etc. change abruptly at the electrode-separator boundary. The insert in Fig. 10 shows the numerical solution of a change of voltage and mean $NaHCO_3$ concentration in time.

Fig. 10 illustrates theoretical and experimental galvanostatic curves of electrode charging. The C^S_{EDL} values in Table 2 were used for calculations. Theoretical and experimental data demonstrate good coincidence. For instance, we can compare the curves for the VISKUMAK and SAIT electrodes, which were obtained for the similar $NAHCO_3$ solution. A slope of the curve for the VISKUMAK electrode is much less indicating its higher capacitance due to higher hydrophilic porosity (see Table 1). Here, the power–law relationship of the coefficient of effective conductivity and effective diffusion coefficient on hydrophilic porosity follows the Archie's law (see Eq. (3)).

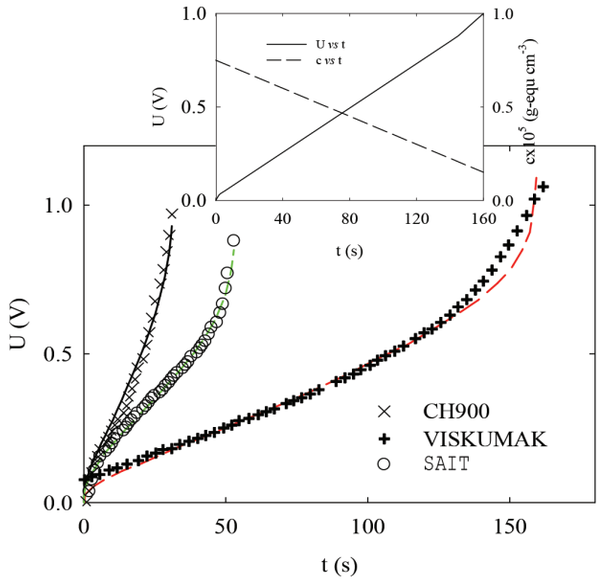

Fig. 10. Experimental (symbols) and theoretical (lines) galvanostatic charging curves for different electrodes. A mixed solution containing $CaCl_2$. $NaHCO_3$ and $MgSO_4$ (CH900) as well as a 0.1 N $NaHCO_3$ solution (VISKUMAK, SAIT) were used, I = 2.8 (a–e) and 10 (f) mA cm^{-2}. Insert: numerical solution of voltage and mean $NaHCO_3$ concentration vs. time.

3.5. Mathematical modeling of a dynamic CDI cell

A scheme of electrochemical components of the dynamic CDI cell is shown in Fig. 11. This is a 2D model with double distributed parameters through porous electrodes and separator.

The main plane of the model is in the r plane. Direction z is perpendicular to the electrode planes. This model is been based on the following assumptions: (i) convective diffusion of the electrolyte can be described by the average equations of mass-transfer based on the dilute-solution theory in porous media; (ii) hydrodynamic velocity is nonzero only in the r-direction; (iii) the effective diffusion coefficients and effective electrolyte conductivity are calculated using the Archie's law (see Eq. (3)); (iv) the electrolyte can be presented as a binary one with an effective concentration [g mol^{-1}] (a difference in transfer numbers can be neglected in this way), (v) the overall conductivity is a sum of electrolyte conductivity, which is a linear function of concentration, and SC [8]; (vi) diffusion can be neglected in all directions except x-direction (there is a marginal hydrodynamic flow in this direction), (vii) the EDL capacitance of the electrode is constant (it is not affected by potential, as shown in Section 3.3). Assumptions (i), (iii) and (iv) are widely used for the mass transfer problems, particularly for those in porous media [55]. Assumption (ii) means independence of viscosity and density of the solution on its concentration. Assumption (vii) is usual; for instance, it was used in [34,35,48,56].

The equations for potential and concentration in the electrode region are:

$$C_s \frac{\partial \varphi - \varphi_C}{\partial t} = \frac{1}{r}\frac{\partial}{\partial r}\left(r\kappa_E \frac{\partial \varphi}{\partial r}\right) + \frac{\partial}{\partial z}\left(\kappa_E \frac{\partial \varphi}{\partial z}\right) \quad (9)$$

$$\varepsilon_E \frac{\partial c}{\partial t} + v_r \frac{\partial c}{\partial r} = D_E\left(\frac{1}{r}\frac{\partial}{\partial r}\left(r\frac{\partial c}{\partial r}\right) + \frac{\partial^2 c}{\partial z^2}\right) + \frac{C_s}{z_+ F} A_E \frac{\partial \varphi - \varphi_C}{\partial t} \quad (10)$$

where C_S is the specific capacitance, φ_C is the electrode potential, φ is the electrolyte potential, t_+ and t_- are the cation and anion transfer numbers, ε_E is the porosity of the electrodes, $\kappa_E = \kappa_{E\lambda}\, c + \kappa_{surf}$ is the electrolyte conductivity in the electrodes, $\kappa_{E\lambda}$ is the reference electrolyte conductivity in electrode, κ_{surf} is the SC of the electrode, $D_E = D_0 \varepsilon_E^{\,n}$ is the

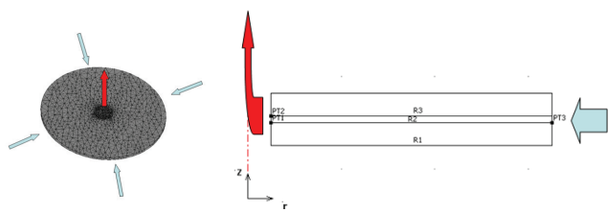

Fig. 11. 2D model of dynamic CDI cell with axial symmetry.

Table 5
Parameters of the dynamic model for the CH900 electrode in the mixed solution

L_E (m)	L_S (m)	C_S (F m^{-3})	κ_E (Ohm^{-1} m^{-1})	κ_S (Ohm^{-1} m^{-1})	κ_M (Ohm^{-1} m^2 mol^{-1})	D (m^2 s^{-1})	ε_E	ε_S	R_{out} (m)	R_{in} (m)	V (m^3 s^{-1})
0.0005	0.00014	15×10^6	0.5	10^{-3}	10^{-7}	1.2×10^{-9}	0.8	0.8	0.065	0.0075	0.333×10^{-6}(a), 0.667×10^{-6}(b)

effective diffusion coefficient of electrolyte in the electrode (exponent n is defined by the properties of porous media), $A_E = \left(t_+ \frac{dq_+}{dq} + t_- \frac{dq_-}{dq} \right) \approx \pm \frac{1}{2}$ is the electric adsorption coefficient [57], v_r is the hydrodynamic velocity in the r-direction.

Thus, taking into consideration Eqs. (2), (4) and (7), the efficiency of the CDI processes depends on EDL characteristics through both the EDL capacitance and SC.

The equations in the spacer region can be written as:

$$\frac{1}{r}\frac{\partial}{\partial r}\left(\kappa_s \frac{\partial \varphi}{\partial r} \right) + \frac{\partial}{\partial z}\left(\kappa_s \frac{\partial \varphi}{\partial z} \right) = 0 \tag{11}$$

$$\varepsilon_S \frac{\partial c}{\partial t} + v_r \frac{\partial c}{\partial r} = D_S \left(\frac{1}{r}\frac{\partial}{\partial r}\left(r \frac{\partial c}{\partial r} \right) + \frac{\partial^2 c}{\partial z^2} \right) \tag{12}$$

where ε_s is the spacer porosity, $\kappa_S = \kappa_{S\lambda}\, c$ is the electrolyte conductivity in the spacer, $\kappa_{E\lambda}$ is the reference electrolyte conductivity in the spacer, $D_S = D_0 \varepsilon_S^{\,n}$ is the effective diffusion coefficient of electrolyte in the spacer.

The r-component of hydrodynamic velocity is present by this equation:

$$v_r = \frac{R_{out} v_i}{r} \tag{13}$$

where R_{out} is the outer radius of the cell, v_i is the velocity in the media, i corresponds to the electrode (i) or spacer (s). There is a trivial relationship between full flow rate V_{min} [ml/min] and these velocities:

$$V_{min} = 2\pi r (2 v_e L_e + v_s L_s) \tag{14}$$

where L_e and L_s are the thicknesses of the electrode and spacer, respectively.

In addition, the fraction of electrolyte flowing through the spacer can be defined as:

$$\alpha = \frac{v_s L_s}{(2 v_e L_e + v_s L_s)} \tag{15}$$

For potential and the concentration, there are the usual conditions of continuity between the spacer and electrodes.

For one electrode boundary (z = down edge), the conditions can be written as:

$$\left.\frac{\partial c}{\partial z}\right|_{z=0} = 0, \quad \left.\frac{\partial \varphi}{\partial z}\right|_{z=0} = 0 \tag{16}$$

$$\left.\varphi_c\right|_{z=0} = 0 \tag{17}$$

For other electrode boundary (z = upper edge), the conditions are:

$$\left.\frac{\partial c}{\partial z}\right|_{z=2L_e+L_s} = 0, \quad \left.\frac{\partial \varphi}{\partial z}\right|_{z=2L_e+L_s} = 0 \tag{18}$$

$$\left.\varphi_c\right|_{z=2L_e+L_s} = U(t) \tag{19}$$

where $U(t)$ is the applied voltage.

For concentration and potential, there should be insulation conditions at the other boundaries except in the inlet zone (where the concentration should be constant) and outlet zone (free condition).

3.6. Calculations according to the dynamic model

The calculation has been carried out using the COMSOL Multiphysics FemLab3.5 software [58]. The stabilization procedure used was the Artificial diffusion (the set of Isotropic diffusion, Streamline diffusion and Crosswind diffusion). The parameters for calculations are given in Table 5.

As an example, Fig. 12 illustrates concentration fields for different time from the process beginning and for various thickness of the separator.

3.7. CDI processes in a dynamic cell: effect of operation conditions. Experiment vs. theory

Theoretical and experimental data calculated for the cell with CH900 electrodes according to the dynamic CDI model are plotted in Fig. 13. As can be seen, the curves are close to each other. A certain divergence of these plots in the region of 0–15 s is evidently due to contact resistances in the cell. It is difficult to take them into consideration. A good agreement between the curves allows assuming correctness of the dynamic model, which can be used further for optimization of CDI processes.

4. Conclusions

As found using MSCP, porous structure and hydrophilic-hydrophobic properties of the composite and textile carbon electrodes are rather different. Very high values of total specific surface area (600–1,520 m^2 g^{-1}), hydrophilic surface area (416–850 m^2 g^{-1}), total porosity (0.71–0.85 cm^{3}cm^{-3}) have been found. At the same time, hydrophilic porosity reaches 0.49–0.79 cm^{3}cm^{-3}, hydrophobic porosity is much lower (0.06–0.22).

The values of EDL capacitance of the activated carbon electrodes have been obtained using a static electrochemical

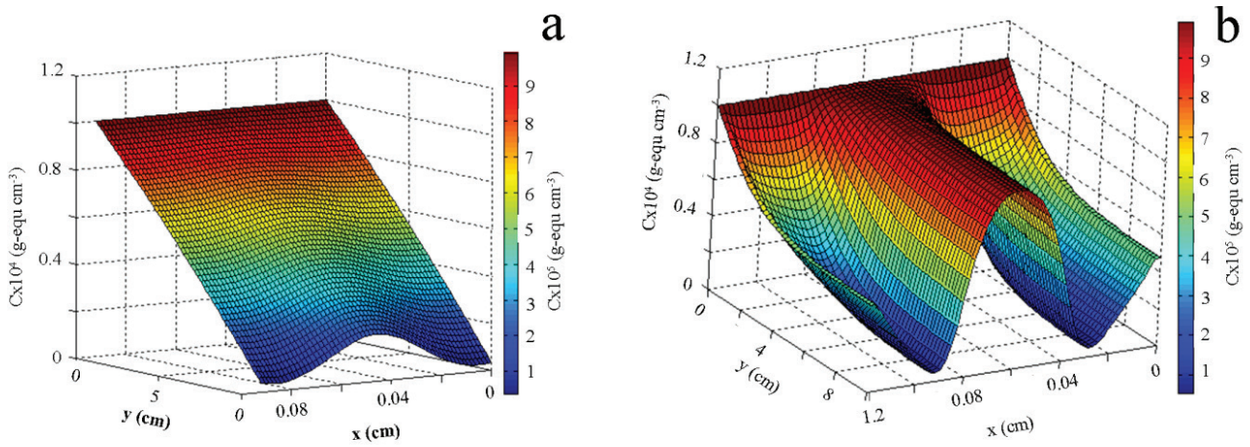

Fig. 12. Concentration field calculated according to the dynamic model: a – v = 0.1 cm s^{-1}, L_s = 0.0120 cm, t = 100 s; b – v = 0.2 cm s^{-1}, L_s = 0.04 cm, t = 5 s. The calculations were performed for the CH900 electrodes in the mixed solution.

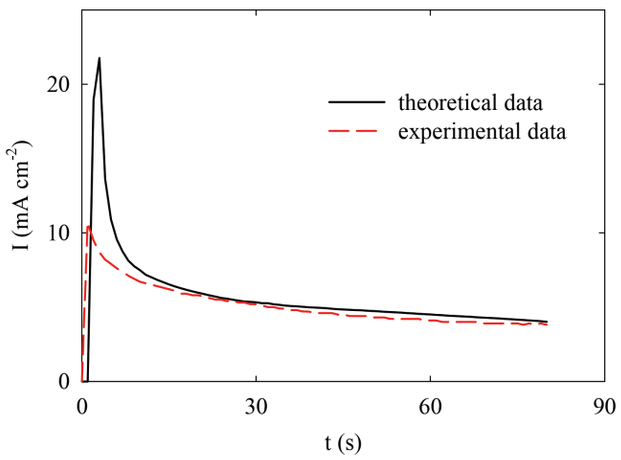

Fig. 13. Comparison of the calculated and experimental dependences of current density on time. U = 1.25 V; the flow rate was 40 cm^3 min^{-1}. The calculations were performed for the CH900 electrodes in the mixed solution.

cell. These values correlate with the porous structure characteristics determined using MSCP. The highest values of specific EDL capacitance (85 and 110 F g^{-1} for solutions containing 100 mg-eq dm^{-3} KCl and $NaHCO_3$ respectively) have been found for the CH900 electrode due to maximal value of hydrophilic surface area (850 m^2 g^{-1}) and hydrophilic porosity (0.76 cm^3 cm^{-3}). The SAIT electrode demonstrates the lowest capacitance values, for instance, 52 F g^{-1} for KCl solution (100 mg-eq dm^{-3}). This is evidently caused by the lowest hydrophilic porosity (0.49 cm^3 cm^{-3}) and, as a result, by the lowest electrical conductivity of the solution inside the electrode. The values of specific capacitance (72 F g^{-1} for the solution containing 100 mg-eq dm^{-3} KCl) and hydrophilic porosity (0.62 cm^3 cm^{-3}) for the VISKUMAK electrode occupy the intermediate position.

Under dynamic conditions, the maximal deionization degree (82%) was found for the CH900 electrodes in the solution containing 5 mg-eq KCl. The deionization process is more efficient in the case of 1:1 electrolyte (KCl) than for the mixed solution containing 1:1, 1:2 and 2:2 electrolytes. Deionization is reinforced in the order: SAIT<VISKUMAK<CH900. The order is similar to that for the EDL capacitance, which is due to their porous structure characteristics and hydrophilic-hydrophobic properties. Thus, the results of this work allow selecting carbon materials with the optimal structure and hydrophilic-hydrophobic processes.

Both deionization and concentration in the dynamic cell were improved with an increase in the cell voltage and decrease in the solution flow velocity. The resulting deionization energy was shown to grow at an increase in voltage, while specific energy efficiency is reduced under these conditions. Since the resulting energy decreases due to return of energy to CDI device during the concentration stage, the processes are less energy-intensive as compared with other deionization techniques. Energy consumption for deep water deionization also becomes lower due to SC of carbon electrodes, which is caused by surface groups. Thus the electrodes for CDI processes have to be characterized by considerable SC (high adsorption capacity). SC provides ionic conductivity of carbon electrodes even in very pure water.

The mathematical model of charging-discharging processes has been developed for the static cell; a good agreement between the theoretical and experimental data has been found. Distributions of solution concentration through porous electrodes and separators have been calculated for different times from the beginning of the deionization process.

The 2D mathematical model of a dynamic CDI cell, which takes into consideration adsorption-desorption, ion transport, characteristics of porous structure of the electrodes and separator, SC of the electrodes as well as EDL capacitance (obtained in the static cell), has been developed. It was shown that the characteristics of the CDI processes sufficiently depend on the EDL characteristics. Firstly, the maximal change in the solution concentration during deionization is proportional to the EDL capacitance. Secondly, a possibility to obtain very pure water is determined by SC

of carbon electrodes. The concentration fields across the cell for different times from the beginning of the deionization stage were calculated. The experimental and theoretical data were found to be in a good agreement indicating correctness of the model. This means that the model can in future be applied to optimization of the CDI processes.

Acknowledgements

The work was performed within the framework of the project "Fundamental aspects of capacitive deionization of aqueous solutions" supported by the Russian Foundation of Basic Research (Grant no. 14-03-00082).

Symbols and abbreviations

A_E — Electric adsorption coefficient
c_0 — Initial concentration, mol m^{-3}
c — Concentration, mol m^{-3}
c_s — Specific capacitance per volume unit, F m^{-3}
D — Diffusion coefficient, m^2 s^{-1}
D_0 — Diffusion coefficient in free electrolyte, m^2 s^{-1}
L_e — Electrode thickness, m
L_s — Separator thickness, m
m — Archie's exponent, dimensionless
F — Faraday constant, C mol^{-1}
r — r-coordinate of electrode, m
R_{out} — Outer radius of electrode, m
S — Outline surface area of the electrode, m^2
t — Time, s
t_+ — Cation transport number, dimensionless
t_- — Anion transport number, dimensionless
V — Solution volume, m^3
v — Hydrodynamic velocity, m s^{-1}
U — Cell voltage, V
W_c — Energy recovery of the concentration stage, J
W_d — Energy consumption of the deionization stage, J
W_r — Resulting deionization energy, J
z — Coordinate in z direction, m

Greek

ε — Porosity, dimensionless
θ — Wetting angle for water, dimensionless
κ_{eff} — Effective conductivity, S m^{-1}
κ_λ — Reference conductivity, S m^{-1}/mol
κ_s — Surface conductivity, S m^{-1}
κ_v — Conductivity of electrolyte in the pore center, S m^{-1}
φ — Electrical potential of electrolyte, V
φ_c — Electrical potential of the solid phase, V
χ — Specific energy efficiency

Index

e — Corresponding to the electrode
S — Corresponding to the spacer

Abbreviations

CDI — Capacitive deionization
EDL — Electric double layer
ECSC — Electrochemical supercapacitors
HDCE — Highly dispersive carbon electrodes
MSCP — Method of standard contact porosimetry
PTFE — Polytetrafluorethylene
SC — Surface conductivity

References

[1] Y. Oren, Capacitive deionization (CDI) for desalination and water treatment – past, present and future (a review), Desalination, 228 (2008) 10–29.
[2] F.A. AlMarzooqi, A.A. Al Ghaferi, I. Saadat, N. Hilal, Application of capacitive deionisation in water desalination: a review, Desalination, 342 (2014) 3–15. doi: 10.1016/j.desal.2014.02.031.
[3] Y.S. Dzyazko, Y.M. Volfkovich, L.N. Ponomaryova, V.E. Sosenkin, V.V Trachevskii, V.N. Belyakov, Composite ion-exchangers based on flexible resin containing zirconium hydrophosphate for electromembrane separation, J. Nanosci. Technol., 2 (2015) 43–49.
[4] Ö. Arar, Ü. Yüksel, N. Kabay, M. Yüksel, Various applications of electrodeionization (EDI) method for water treatment – a short review, Desalination, 342 (2014) 16–22.
[5] L. Alvarado, A. Chen, Electrodeionization: principles, strategies and applications, Electrochim. Acta, 132 (2014) 583–597.
[6] Y.S. Dzyazko, L.N. Ponomaryova, L.M. Rozhdestvenskaya, S.L. Vasilyuk, V.N. Belyakov, Electrodeionization of low-concentrated multicomponent Ni 2+-containing solutions using organic–inorganic ion-exchanger, Desalination, 342 (2014) 43–51.
[7] T.J. Welgemoed, C.F. Schutte, Capacitive Deionization Technology™: an alternative desalination solution, Desalination, 183 (2005) 327–340.
[8] Y.M. Vol'fkovich, A.A. Mikhalin, A.Y. Rychagov, Surface conductivity measurements for porous carbon electrodes, Russ. J. Electrochem., 49 (2013) 594–598.
[9] D.-W. Wang, F. Li, Z.-G. Chen, G.Q. Lu, H.-M. Cheng, Synthesis and electrochemical property of boron-doped mesoporous carbon in supercapacitor, Chem. Mater., 20 (2008) 7195–7200.
[10] C.J. Gabelich, T.D. Tran, I.H. Suffet, Electrosorption of inorganic salts from aqueous solution using carbon aerogels, Environ. Sci. Technol., 36 (2002) 3010–3019. doi: 10.1021/es0112745.
[11] C. Nie, L. Pan, H. Li, T. Chen, T. Lu, Z. Sun, Electrophoretic deposition of carbon nanotubes film electrodes for capacitive deionization, J. Electroanal. Chem., 666 (2012) 85–88.
[12] H. Li, T. Lu, L. Pan, Y. Zhang, Z. Sun, Electrosorption behavior of graphene in NaCl solutions, J. Mater. Chem., 19 (2009) 6773–6779.
[13] H. Wang, D. Zhang, T. Yan, X. Wen, J. Zhang, L. Shi, Q. Zhong, Three-dimensional macroporous graphene architectures as high performance electrodes for capacitive deionization, J. Mater. Chem. A., 1 (2013) 11778–11789.
[14] G. Wang, Q. Dong, Z. Ling, C. Pan, C. Yu, J. Qiu, Hierarchical activated carbon nanofiber webs with tuned structure fabricated by electrospinning for capacitive deionization, J. Mater. Chem., 22 (2012) 21819–21823.
[15] A. Amiri, G. Ahmadi, M. Shanbedi, M. Savari, S.N. Kazi, B.T. Chew, Microwave-assisted synthesis of highly-crumpled, few-layered graphene and nitrogen-doped graphene for use as high-performance electrodes in capacitive deionization, Sci. Rep., 5 (2015) 1–13.
[16] A. Aghigh, V. Alizadeh, H.Y. Wong, M.S. Islam, N. Amin, M. Zaman, Recent advances in utilization of graphene for filtration and desalination of water: a review, Desalination, 365 (2015) 389–397.
[17] H. Li, L. Pan, T. Lu, Y. Zhan, C. Nie, Z. Sun, A comparative study on electrosorptive behavior of carbon nanotubes and graphene for capacitive deionization, J. Electroanal. Chem., 653 (2011) 40–44. doi: 10.1016/j.jelechem.2011.01.012.
[18] Z. Peng, D. Zhang, L. Shi, T. Yan, High performance ordered mesoporous carbon/carbon nanotube composite electrodes for capacitive deionization, J. Mater. Chem., 22 (2012) 6603–6612.

[19] M.S. Gaikwad, C. Balomajumder, Polymer coated capacitive deionization electrode for desalination: a mini review, Electrochem. Energy Technol., 2 (2016) 1–5.
[20] Y. Liu, C. Nie, X. Liu, X. Xu, Z. Sun, L. Pan, Review on carbon-based composite materials for capacitive deionization, RSC Adv., 5 (2015) 15205–15225.
[21] Z. Peng, D. Zhang, T. Yan, J. Zhang, L. Shi, Three-dimensional micro/mesoporous carbon composites with carbon nanotube networks for capacitive deionization, Appl. Surf. Sci., 282 (2013) 965–973.
[22] H. Wang, L. Shi, T. Yan, J. Zhang, Q. Zhong, D. Zhang, Design of graphene-coated hollow mesoporous carbon spheres as high performance electrodes for capacitive deionization, J. Mater. Chem. A., 2 (2014) 4739–4750.
[23] X. Wen, D. Zhang, T. Yan, J. Zhang, L. Shi, Three-dimensional graphene-based hierarchically porous carbon composites prepared by a dual-template strategy for capacitive deionization, J. Mater. Chem. A., 1 (2013) 12334–12344.
[24] J.-B. Lee, K.-I.K.-K. Park, S.-W. Yoon, P.-Y. Park, K.-I.K.-K. Park, C.-W. Lee, Desalination performance of a carbon-based composite electrode, Desalination, 237 (2009) 155–161.
[25] D. Zhang, X. Wen, L. Shi, T. Yan, J. Zhang, Enhanced capacitive deionization of graphene/mesoporous carbon composites, Nanoscale., 4 (2012) 5440–5446.
[26] T.-Y. Ying, K.-L. Yang, S. Yiacoumi, C. Tsouris, Electrosorption of ions from aqueous solutions by nanostructured carbon aerogel, J. Colloid Interface Sci., 250 (2002) 18–27.
[27] M.T.Z. Myint, J. Dutta, Fabrication of zinc oxide nanorods modified activated carbon cloth electrode for desalination of brackish water using capacitive deionization approach, Desalination, 305 (2012) 24–30.
[28] L. Han, K.G. Karthikeyan, M.A. Anderson, J.J. Wouters, K.B. Gregory, Mechanistic insights into the use of oxide nanoparticles coated asymmetric electrodes for capacitive deionization, Electrochim. Acta, 90 (2013) 573–581. doi: 10.1016/j.electacta.2012.11.069.
[29] R. Broséus, J. Cigana, B. Barbeau, C. Daines-Martinez, H. Suty, Removal of total dissolved solids, nitrates and ammonium ions from drinking water using charge-barrier capacitive deionisation, Desalination, 249 (2009) 217–223.
[30] S.-J. Seo, H. Jeon, J.K. Lee, G.-Y. Kim, D. Park, H. Nojima, J. Lee, S.-H. Moon, Investigation on removal of hardness ions by capacitive deionization (CDI) for water softening applications, Water Res., 44 (2010) 2267–2275.
[31] H. Li, L. Zou, L. Pan, Z. Sun, Using graphene nano-flakes as electrodes to remove ferric ions by capacitive deionization, Sep. Purif. Technol., 75 (2010) 8–14.
[32] L. Li, L. Zou, H. Song, G. Morris, Ordered mesoporous carbons synthesized by a modified sol-gel process for electrosorptive removal of sodium chloride, Carbon, 47 (2009) 775–781. doi: 10.1016/j.carbon.2008.11.012.
[33] Y.-J. Kim, J.-H. Choi, Selective removal of nitrate ion using a novel composite carbon electrode in capacitive deionization, Water Res., 46 (2012) 6033–6039.
[34] A.M. Johnson, J. Newman, Desalting by means of porous carbon electrodes, J. Electrochem. Soc., 118 (1971) 510–517.
[35] Y.M. Vol'fkovich, V.M. Mazin, N.A. Urisson, Operation of double-layer capacitors based on carbon materials, Russ. J. Electrochem., 34 (1998) 740–746.
[36] K.-L. Yang, T.-Y. Ying, S. Yiacoumi, C. Tsouris, E.S. Vittoratos, Electrosorption of ions from aqueous solutions by carbon aerogel: an electrical double-layer model, Langmuir, 17 (2001) 1961–1969. doi: 10.1021/la001527s.
[37] Y.A.C. Jande, W.S. Kim, Predicting the lowest effluent concentration in capacitive deionization, Sep. Purif. Technol., 115 (2013) 224–230.
[38] Y. a C. Jande, W.S. Kim, Modeling the capacitive deionization batch mode operation for desalination, J. Ind. Eng. Chem., 20 (2014) 3356–3360. doi: 10.1016/j.jiec.2013.12.020.
[39] P.M. Biesheuvel, S. Porada, M. Levi, M.Z. Bazant, Attractive forces in microporous carbon electrodes for capacitive deionization, J. Solid State Electrochem., 18 (2014) 1365–1376. doi: 10.1007/s10008-014-2383-5.
[40] P.M. Biesheuvel, M.Z. Bazant, Nonlinear dynamics of capacitive charging and desalination by porous electrodes, Phys. Rev. E – Stat. Nonlinear, Soft Matter Phys., 81 (2010) 031502–12.
[41] A. Mani, M.Z. Bazant, Deionization shocks in microstructures, Phys. Rev. E – Stat. Nonlinear, Soft Matter Phys., 84 (2011) 61504–13. doi: 10.1103/PhysRevE.84.061504.
[42] P.M. Biesheuvel, Y. Fu, M.Z. Bazant, Electrochemistry and capacitive charging of porous electrodes in asymmetric multicomponent electrolytes, Russ. J. Electrochem., 48 (2012) 580–592. doi: 10.1134/S1023193512060031.
[43] Y.M. Volfkovich, V.E. Sosenkin, V.S. Bagotsky, Structural and wetting properties of fuel cell components, J. Power Sources., 195 (2010) 5429–5441.
[44] Y.M. Volfkovich, V.S. Bagotzky, V.E. Sosenkin, I.A. Blinov, The standard contact porosimetry, Colloids Surfaces A: Physicochem. Eng. Asp., 187 (2001) 349–365.
[45] Y.M. Volfkovich, V.S. Bagotzky, The method of standard porosimetry: 1. Principles and possibilities, J. Power Sources., 48 (1994) 327–338.
[46] Y.M. Volfkovich, I.A. Blinov, V.E. Sosenkin, V.V. Kulbachevsky, Porosimeter, 2001, U.S. patent 6,298,711.
[47] J. Rouquerol, G. Baron, R. Denoyel, H. Giesche, J. Groen, P. Klobes, P.E. Levitz, A.V. Neimark, S. Rigby, R. Skudas, K.S. William Sing, M. Thommes, K.K. Unger, Liquid intrusion and alternative methods for the characterization of macroporous materials (IUPAC Technical Report), Pure Appl. Chem., 84 (2011) 107–136.
[48] B.E. Conway, Electrochemical Supercapacitors: Scientific Fundamentals and Technological Applications, Springer, 1999.
[49] Y.M. Volfkovich, D.A. Bograchev, A.A. Mikhalin, V.S. Bagotsky, Supercapacitor carbon electrodes with high capacitance, J. Solid State Electrochem., 18 (2013) 1351–1363.
[50] Y.M. Volfkovich, D.A. Bograchev, A.Y. Rychagov, V.E. Sosenkin, M.Y. Chaika, Supercapacitors with carbon electrodes. Energy efficiency: modeling and experimental verification, J. Solid State Electrochem., 19 (2015) 2771–2779.
[51] Y.A. Chizmadzhev, V.S. Markin, M.R. Tarasevich, Y.G. Chirkov, J.J. Bikerman, Macrokinetics of Processes in Porous Media (Fuel Cells), Nauka, Moscow, 1971.
[52] G.E. Archie, Classification of carbonate reservoir rocks and petrophysical considerations, Am. Assoc. Pet. Geol. Bull., 36 (1952) 278–298.
[53] I.G. Gurevich, U.M. Volfkovich, V.S. Bagotskli, Liquid Porous Electrodes, Nauka Technika, Minsk, 1974.
[54] J. Newman, K.E. Thomas-Alyea, Electrochemical Systems, John Wiley & Sons, 2004.
[55] J. Newman, W. Tiedemann, Porous electrode theory with battery applications, AIChE J., 21 (1975) 25–41.
[56] B. Pillay, J. Newman, The influence of side reactions on the performance of electrochemical double layer capacitors, J. Electrochem. Soc., 143 (1996) 1806–1814.
[57] A.M. Johnson, J. Newman, Desalting by means of porous carbon electrodes, J. Electrochem. Soc., 118 (1971) 510–517.
[58] COMSOL Multiphysics, Modeling Guide, Version 3.5a, COMSOL AB, Burlington, MA, 2008.